Published in ACS Applied Nano Materials (*ACS Appl. Nano Mater.* 2021, 4, 11, 11466-11472)

Direct Synthesis of Sulfide-Capped Nanoparticles for Carbon-Free Solution Processed Photovoltaics

Ryan G. Ellis, Swapnil D. Deshmukh, Jonathan W. Turnley, Dwi S. Sutandar, Jacob P. Fields, and Rakesh Agrawal*

Davidson School of Chemical Engineering, Purdue University, West Lafayette, IN 47907, USA

*Corresponding Author: agrawalr@purdue.edu

Abstract

Colloidal nanoparticles have demonstrated significant promise in the fabrication of solution-processed $Cu(In,Ga)(S,Se)_2$ photovoltaics. However, carbonaceous impurities from long-chain native ligands retained in the films during and after heat treatments have necessitated the exploration of post-synthetic ligand exchange procedures, which increases process complexity, solvent usage, and could potentially reduce the cost advantages solution processing aims to deliver over conventional vacuum processing. In this report, a new method to directly synthesize anion impurity-free $CuInS_2$ nanoparticles with both inorganic and thermally degradable thioacetamide ligands is developed to bypass the need for ligand exchange completely. Metal thiolate complexes were isolated from solutions of Cu_2S or Cu, and In precursors in amine-thiol mixtures. The isolated metal thiolate complexes were solubilized in the readily available and low toxicity solvent, sulfolane, and were thermally decomposed to $CuInS_2$ nanoparticles in presence of thioacetamide. H_2S formed during thiolate decomposition was used in conjunction with thioacetamide as ligands for nanoparticles. High mass concentration inks in the low toxicity polar solvent, dimethyl sulfoxide, was used to easily deposit thin films using scalable blade coating. $CuInSe_2$ photovoltaic device with total area power conversion efficiency of 7.1% was prepared from carbon-free $CuInS_2$ nanoparticle film. Further, the synthetic methods were successfully adapted to the more complex quaternary material, Cu_2ZnSnS_4 where phase pure material synthesis was observed. The developed methods represent a paradigm shift in the synthesis of metal sulfide nanomaterials and the subsequent solution processing of photovoltaics without the need for ligand exchange.

Keywords: Nanoparticles, nanocrystals, ligand, chalcogenide, photovoltaic, thioacetamide, thiolate

$Cu(In,Ga)(S,Se)_2$ (CIGSSe) has proven to be a robust absorber layer for thin-film photovoltaics, reaching champion power conversion efficiencies up to 23.35% on the lab scale via vacuum processing.[1] However, CIGSSe has historically relied on batch processing with vacuum-based deposition, which limits manufacturing throughput, lacks large area uniformity, and requires costly equipment. Solution processing has emerged as an alternative fabrication technique that bypasses vacuum processing, allowing for roll-to-roll compatible, atmospheric pressure, liquid phase deposition. Solution-processed CIGSSe has reached champion power conversion efficiencies of 18.1 % (17.2% certified) using a hydrazine molecular precursor system by solubilizing Cu_2S, In_2Se_3, Ga, S, and Se.[2] A major advantage of the hydrazine system is the clean thermal decomposition of the precursor solutions into CIGSSe without oxygen, anion, and carbon impurities. However, a major limitation of this system is the highly explosive and carcinogenic properties of hydrazine, placing a major hurdle on the path to large-scale manufacturing.[3] As such, numerous hydrazine-free solution processing routes have been explored, either through molecular precursors,[4–9] or colloidal nanoparticles.[10–17] Of solution processing techniques, colloidal nanoparticle inks have emerged as a versatile, low-toxicity method for chalcogenide thin film deposition, reaching the total area power conversion efficiencies of 15%.[11] However, a persisting limitation of nanoparticle approaches is the carbonaceous impurities imparted by native ligands, generally long-chain alkylamines such as oleylamine.

These long-chain ligands are used for their high boiling point, ability to control reaction kinetics, and nanoparticle morphology while providing high colloidal stability.[18,19] However, these ligands pyrolyze into graphitic carbon when annealed in inert atmospheres[20] and react with selenium during the selenization process, leaving a discrete segregated carbonaceous impurity layer at the back contact.[13,17,21] This impurity layer can limit the ultimate thickness of the coarsened grains, affect elemental distribution,[22] and potentially increase series resistance.

As a method to remove these native ligands, ligand exchange reactions have drawn significant interest. By a post-synthesis replacement of the long-chain carbonaceous ligands with either volatile organics,[23–25] or non-contaminating inorganic species,[26,27] low-carbon nanoparticle thin films can be produced while retaining the benefits of the long-chain ligands during synthesis. In our recent report,[17] we detailed a method whereby tightly bound oleylamine ligands on $Cu(In,Ga)S_2$ nanoparticles were removed via a two-step, hybrid organic/inorganic exchange with pyridine and diammonium sulfide. After ligand exchange, greater than 98% of the native ligands were successfully removed and highly stable sulfide capped nanoparticle inks were formulated in dimethyl sulfoxide (DMSO) solvent. Selenization of ligand exchanged nanoparticle films exhibited significantly improved grain growth with little to no fine-grain layer, and improved device performance as compared to an identically fabricated device from oleylamine capped nanoparticles.[17] However, the ligand exchange process requires many additional processing steps and increases solvent usage substantially for the generally low mass concentration exchange steps,[17,27] hindering the potential cost advantage and simplicity solution processing aims to deliver. Several reports have attempted to synthesize nanoparticles that do not require post-synthetic ligand exchange using metal salts in glycol,[28] or metal salts in formamide with thioacetamide as a sulfide source.[29] However, in the case of glycol, formation of secondary oxide phases,[28] surface oxidation during synthesis, or alkoxide ligand binding and decomposition can detriment device performance.[30] Further, poor colloidal stability from this method requires the addition of polymeric dispersants such as polyvinylpyrrolidone (PVP), which again introduces substantial carbon contamination.[28] Others have made use of low-temperature syntheses from solubilized metal chalcogenide complexes, but resultant device performance remained poor.[31]

In this report, we develop a method to bypass the long-standing necessity and extra complexity of carbon impurity removal through ligand exchange reactions by the direct synthesis of $CuInS_2$ (CIS) nanoparticles with a combination of inorganic sulfide ligands and thermally degradable thioacetamide ligands. To ensure high quality of nanoparticles without any anionic impurities, Cu_2S or Cu with In metal were solubilized as precursors in amine-thiol mixtures removing anionic impurity concerns as described in our previous report.[14] Excess amine and thiol were removed[7] and isolated metal thiolate complexes then thermally decomposed via a hot injection reaction in sulfolane which acts as a non-binding polar-aprotic solvent with a thioacetamide and in-situ generated H_2S as a sulfide ligand source. The resulting CIS nanoparticles were phase pure chalcopyrite and exhibited high colloidal stability in polar solvents such as DMSO. Inks with mass concentrations up to 225 mg/mL were prepared and highly uniform and crack free thin films were easily deposited using scalable blade coating and finished into $CuInSe_2$ photovoltaic devices, reaching power conversion efficiencies of 7.1% demonstrating the promise of the ligand exchange free CIS nanoparticle synthesis method. With the methods developed in this report, the need for cumbersome ligand exchange processes is completely bypassed, simplifying solution processing of photovoltaics with colloidal nanoparticles.

Cu_2S or Cu metal along with In metal were selected as precursors due to their ease of reactive dissolution in monoamine-dithiol mixtures. Separate Cu_2S and In solutions or a single solution of Cu and In were prepared in propylamine/1,2-ethanedithiol mixtures. Within 12 hours, complete dissolution of the solids was observed at room temperature yielding homogenous and transparent precursor solutions of metal thiolate complexes.[7] The thermal decomposition of these species was investigated in our previous report, where only metal sulfides and volatile by-products (ethylene sulfide, alkylamine, and hydrogen sulfide) formation was observed (Scheme 1).[14] This removes the concern of anionic impurities typically present with the use of metal salts such as metal acetates, acetylacetonates, nitrates, halides, etc.,[18,19] which can bind to nanoparticle surfaces as ligands or directly incorporate into the crystal structure of the targeted material.[32] While anionic impurities are removed in this method, amines and thiols are known to bind strongly as either

L-type ligands (donation of two electrons from a neutral species to a cationic metal) or X-type ligand (donation of one electron from an anionic species to a cationic metal).[33] As such, isolation of the metal thiolate species from the bulk amine-thiol mixtures was performed to remove all free amine and thiol from the precursor, yielding isolated powder of copper and indium thiolate complexes as was explored in our previous report.[7]

The isolated metal thiolate precursor solids were readily soluble in a wide variety of polar solvents. However, careful selection of a reaction solvent was necessary to ensure a high boiling point for synthesis, thermal stability, low reactivity with reaction mixture constituents, solubilization of all precursors, and sufficient polarity to disperse sulfide capped particles. Importantly, the bulk solvent should not bind to the nanoparticle surface as a ligand, introducing additional carbonaceous species that would necessitate removal. As such, aprotic solvents were initially selected to prevent the strong X-type ligand-binding mechanism from occurring that has been observed for protic species such as alcohols.[30] Sulfolane emerged as an attractive solvent option with relatively low toxicity, good thermal and chemical stability at a variety of acidic and basic conditions, high polarity ($\mu = 4.7$ debye, $\varepsilon = 43.4$), and availability at high purity (>99%) and low cost due to existing commercial use in the petrochemical industry for aromatics extractions and sour gas sweetening.[34–36]

An inorganic sulfide ligand was targeted during the synthesis, and thus required a sulfide source. Conveniently, during the decomposition of the metal thiolate precursor complexes, H_2S gas is liberated into the reaction mixture as a by-product, thus providing a source of potential H-S-Metal X-type ligand, or H_2S L-type binding, similar to the stabilization mechanism that diammonium sulfide uses via electrostatic repulsion.[14,17] However, this H_2S alone was not enough to properly stabilize the nanoparticles. As thioacetamide (TAA) undergoes slow thermal decomposition beginning at around 180°C in an inert environment forming H_2S and acetonitrile (b.p. 82°C),[29] it was added as an additional ligand to the reaction mixture (Scheme 1).

Scheme 1. Reaction pathway illustrating formation of sulfide capped $CuInS_2$ nanoparticles starting from elemental metal precursors

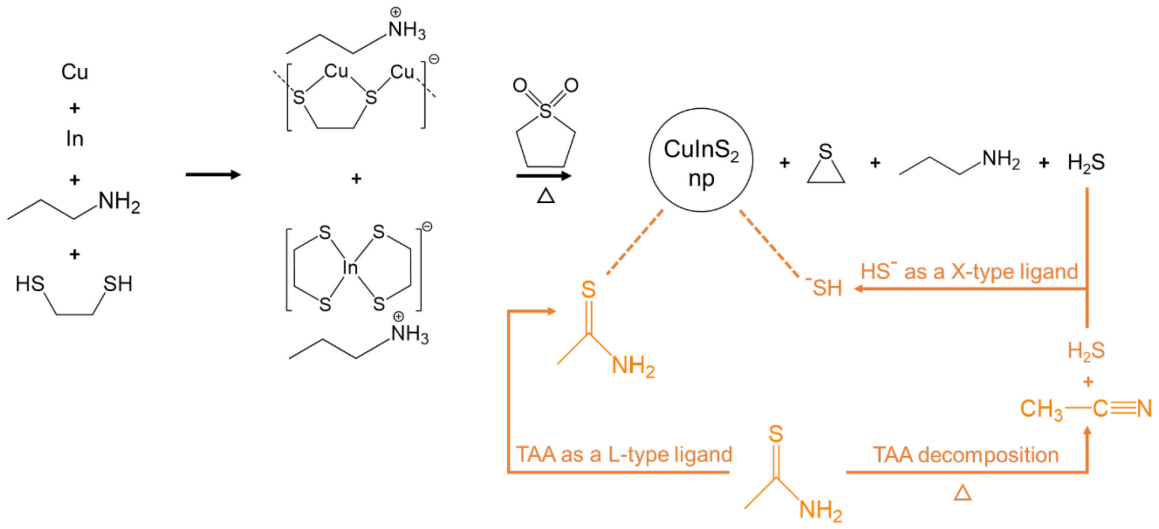

A hot injection reaction was used for nanoparticle synthesis. Due to slightly different reactivities observed for Cu/In precursors and Cu_2S/In precursors, reaction times of 200°C/15 minutes and 210°C/30 minutes were used respectively to obtain particles with the correct stoichiometry. Considering sulfolane's miscibility with non-polar aromatic organics, toluene was selected as an antisolvent for nanoparticle washing with centrifugation to separate the particles. After decanting the supernatant, acetonitrile was used to disperse the nanoparticles for subsequent washes. Four total washes were used to exhaustively remove any residual reaction mixture as determined by ^{1}H-NMR, followed by drying with flowing argon at room

temperature. The use of non-coordinating washing solvents such as acetonitrile and toluene further aids in the prevention of impurity oxide formation from alkoxide binding which can occur during washing with alcohols.[30]

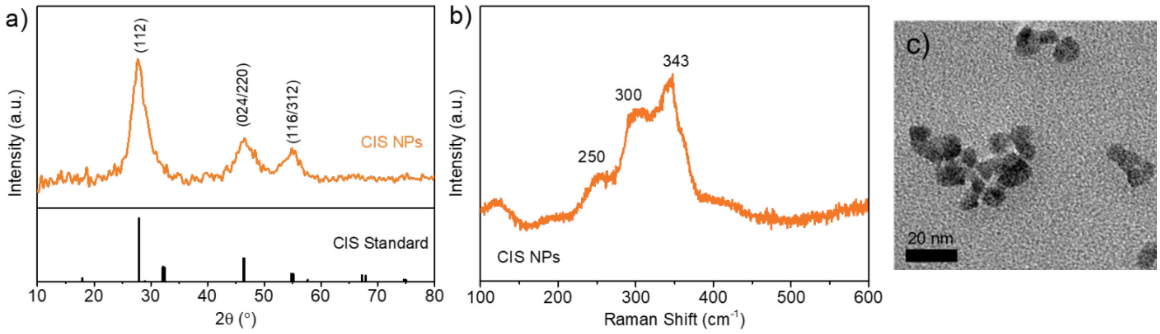

Figure 1. a) XRD, b) Raman, and c) TEM of CIS nanoparticles synthesized from Cu and In metals. Chalcopyrite phase CIS PXRD standard from ICSD collection code 186714

The resulting nanoparticles exhibited a chalcopyrite phase and did not contain any crystalline or amorphous secondary phases, as determined by XRD and Raman as shown in Figures 1a and 1b.[37] Average particle size of approximately 8 nm was observed in transmission electron microscopy as shown in Figure 1c. High resolution TEM of nanoparticles synthesized from Cu_2S and In are shown in Figure S1. XRF revealed a Cu/In ratio of 0.95, slightly above the Cu/In of 0.92 in the precursor solution used for nanoparticles synthesized from both Cu and Cu_2S as copper precursors. Absorption signature for particles synthesized using Cu precursor was collected using UV-vis spectroscopy which showed lowest bandgap at approximately 1.6 eV which is close to the bulk band gap of 1.55 eV reported for $CuInS_2$ material. However, some variation observed in the bandgap can be attributed to the polydispersity and the resulting confinement of the synthesized nanoparticles (Figure S2). To determine the ligand shell of the nanoparticles, ^{1}H-NMR and FTIR were employed. Qualitative ^{1}H-NMR of the CIS nanoparticles, thioacetamide, and sulfolane standards are shown in Figure 2, where all sharp peaks can be attributed to the DMSO-d6 residual, and trace amounts of the washing solvents toluene and acetonitrile. All water seen in Figure 2a is attributed to impurities in the deuterated DMSO (Figure S3).

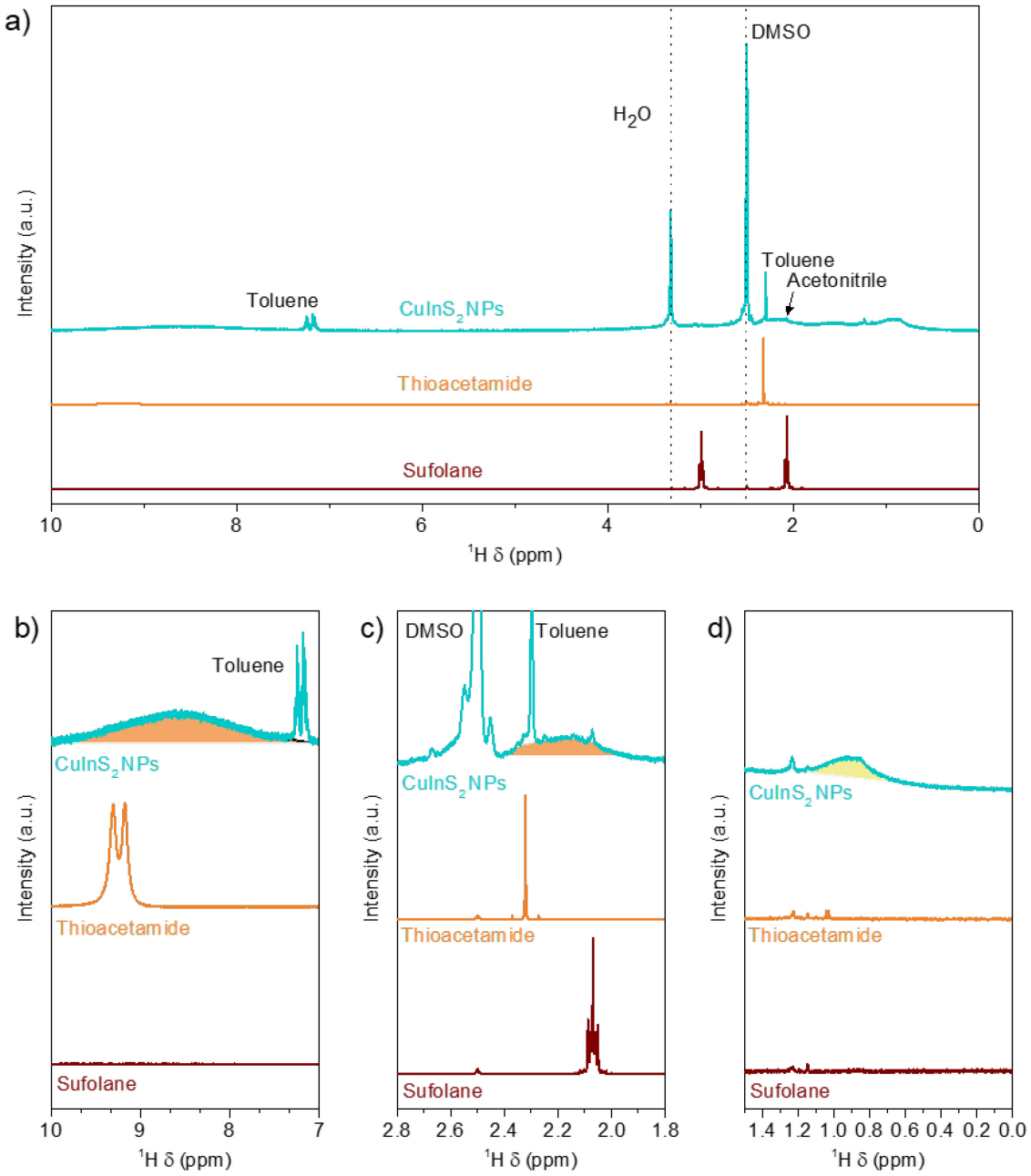

Figure 2. a) Full spectrum ^{1}H-NMR of neat sulfolane, thioacetamide, and CIS nanoparticles synthesized from Cu and In precursors. Zoom-in of the region from b) 7 to 10 ppm, c) 1.8 to 2.8 ppm, and d) 0 to 1.5 ppm. Hypothesized broad peaks assigned to bound thioacetamide are shown in orange and the hypothesized surface H-S-/H_2S peak is highlighted in yellow. Note that intensity is not quantitative, Y-scaling is performed per curve and per panel for clarity.

Three broad peaks observed across the spectrum are indicative of surface-bound species due to surface immobilization, causing peak shift and broadening. Zoomed in ^{1}H-NMR spectra around each of the broadened peaks are shown in Figures 2b, 2c, and 2d. The broad peaks centred at 8.57 ppm and 2.19 ppm are attributed to thioacetamide's NH_2 and CH_3 protons respectively, shifted to lower ppm as is often observed for ligand peak shift in other systems.[38] While there is a literature suggesting possible reaction between thioacetamide and amine forming a product which could act as a ligand through the S atom, the

low boiling point of propylamine (b.p 45 °C) compared to relatively hot reaction mixture (200-210 °C) and the absence of any amine protons in ^{1}H-NMR suggests less likelihood for such reactions.[39] Diammonium sulfide capped CIGS nanoparticles prepared by ligand exchange from the method described from our previous work are shown in Figure S4 and are characteristically missing the peaks assigned to thioacetamide, supporting the hypothesized assignments.[17] The broad peak centred around 0.9 ppm is hypothesized to be X-type surface H-S- or L-type H_2S. Generally, the H-S on thiols is observed as low as 1.2 ppm. The lower shift observed in Figure 2d is likely due to bound surface immobilization. The other peaks observed in Figure 2d are attributed to trace impurities in the deuterated DMSO, as evidenced by their appearance in all spectra. All broad peaks have extremely low intensities, as is expected for bound short-chain species, where peaks corresponding to the protons closest to the bound groups broaden the most significantly.[17] The lack of any appreciable sharp signals of sulfolane and thioacetamide in the nanoparticle spectrum verify that the washing is sufficient to remove all unreacted precursors and reaction solvent. To further investigate carbon content in films fabricated from these particles, transmission FTIR was performed on films blade coated from a DMSO ink at 200 mg/mL concentration on soda-lime glass near C-H region (where soda-lime glass is IR transparent). These films were dried at 100°C for 5 minutes to remove residual coating solvent and then annealed at 320°C (the temperature used for annealing between coatings in later device fabrication) for 5 minutes in a nitrogen atmosphere. Because the blade coated film was uniform in thickness (Figure S5), direct comparison can be made between the pre-annealed and post-annealed films due to identical path length across the thickness of the film as shown in Figure 3.

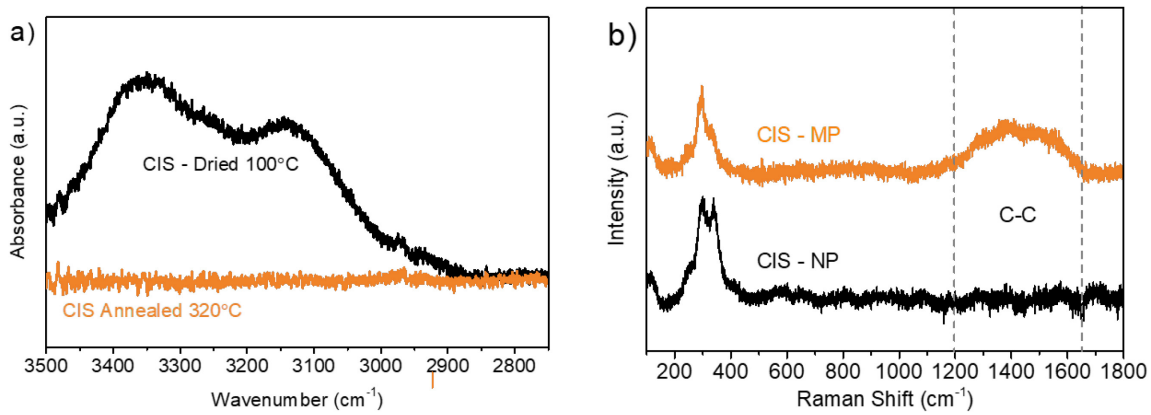

Figure 3. a) FTIR on CIS nanoparticles from Cu_2S and In precursors before and after annealing at 320°C, showing removal of surface-bound thioacetamide from the annealed film b) Raman spectroscopy showing the graphitic carbon-carbon region of CIS nanoparticles annealed at 320°C (CIS-NP) compared to a molecular precursor film from Cu_2S and In in n-butylamine/1,2-ethanedithiol solution annealed at 300°C (CIS-MP).

In the pre-annealed film, several broad peaks, attributed to amide (3100-3500 cm^{-1}), and small C-H stretches (~2950 cm^{-1}) are observed. These peaks are assigned to thioacetamide; however, the observed broadening suggests thioacetamide is surface bound. While the nanoparticle synthesis reaction was performed at 200-210°C above the thermal decomposition onset of thioacetamide at 180°C, incomplete decomposition of the large excess of thioacetamide can facilitate L-type ligand surface binding. After annealing at 320°C, all signals are removed to the detection limit of FTIR, verifying a clean decomposition of surface-bound thioacetamide and an easy method to obtain carbon free nanoparticle thin films. Full spectrum FTIR is shown in Figure S6, where a film was dropcast from acetonitrile and annealed at 150°C, below thioacetamide's decomposition onset but well above acetonitrile's boiling point. Broad amide and C-H stretches are observed, attributed to residual surface thioacetamide. Removal of thioacetamide by the 320 °C annealing temperature was further confirmed by thermogravimetric analysis (TGA) as shown in Figure S7, where a distinct mass loss onset at approximately 180°C and ending at 320°C is observed. Due to absence of C-H signals by FTIR and C-C signals by Raman after 320°C, additional mass loss observed on TGA is thought to be loss of sulfur from the $CuInS_2$ nanoparticles. Further analysis was performed using

Raman spectroscopy to probe any residual C-C bonds, which often occur from coke like pyrolysis by-products and are relatively hard to detect in FTIR. Films from the nanoparticle synthesis were compared to films directly cast from molecular precursors of Cu_2S and In thiolate precursors in amine-thiol solution. Interestingly, significant C-C bonding is observed from the molecular precursor, but not in the case of the sulfide capped nanoparticles, potentially providing a method to bypass carbon impurities often observed from molecular precursor approaches from either metal thiolate decomposition or bulk amine and thiol decomposition.[6]

Nanoparticles inks were easily prepared at mass concentrations exceeding 200 mg/mL in DMSO. DMSO was selected due to its low toxicity as well as its lack of oxide-inducing ability as demonstrated in our previous work.[17] Using blade coating on a preheated substrate at 80°C, high-quality thin films were prepared with a low surface roughness as shown in Figure S5. Films were free of any microcracks as shown in the plan-view SEM image in Figure S8. Sodium fluoride was evaporated onto the films as an extrinsic dopant and selenization was performed in a tubular furnace with selenium pellets at 500°C. The selenized films were finished into complete devices with a chemical bath deposition of a CdS buffer layer (50nm), sputtered i-ZnO (80nm) and indium doped tin oxide (ITO) (220nm) as a transparent conducting oxide (TCO) along with electron beam evaporated Ni/Al grids and anti-reflective MgF_2 layer. A cross-section SEM image for this complete device is shown in Figure S9. A total area power conversion efficiency of 7.1% was obtained for $CuInSe_2$ device fabricated using the direct sulfide capped nanoparticles as shown in Figure 4a. The bandgap of 1 eV was obtained for the selenized material using external quantum efficiency data in Figure 4b which matches the reported value for $CuInSe_2$ material in the literature. While it is a promising performance of 1 eV bandgap material, optimization with film thickness, Na addition, and selenization conditions has the potential to further improve this performance.

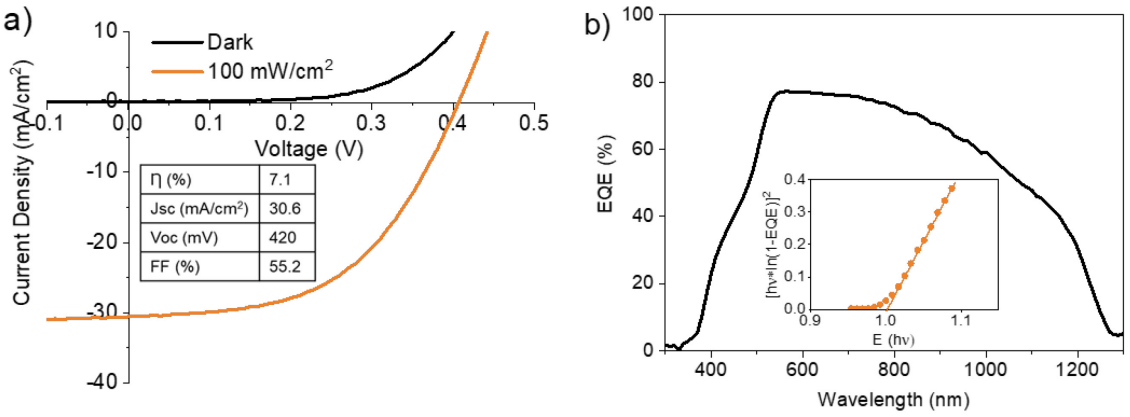

Figure 4. a) Current-voltage analysis and b) external quantum efficiency (EQE) analysis of $CuInSe_2$ solar cell fabricated from direct sulfide capped $CuInS_2$ nanoparticles from Cu and In precursors.

To further explore the potential of this system, the significantly more complex quaternary material, Cu_2ZnSnS_4 (CZTS), known for its difficulty of synthesis and ease of secondary phases formation,[40] was prepared by first dissolving Cu, Zn, and Sn metals in propylamine/1,2-ethanedithiol solutions followed by isolation of the thiolate complexes. The resulting complexes showed lower solubility in sulfolane than their CIS counterpart, so propylamine was used in a small quantity to increase the solubility of the complexes in the sulfolane. Again, hot injection into thioacetamide containing sulfolane at 200°C was performed. XRD pattern collected on these particles shown in Figure 5a confirmed the formation of wurtzite phase CZTS nanoparticles, matching previously reported wurtzite CZTS nanoparticles from a metal salt, sulfur, and oleylamine reaction.[41] Raman spectroscopy performed on these particles (Figure 5b) also showed a strong peak at 334 cm^{-1} which is a characteristic of A mode in wurtzite CZTS nanoparticles.[42]

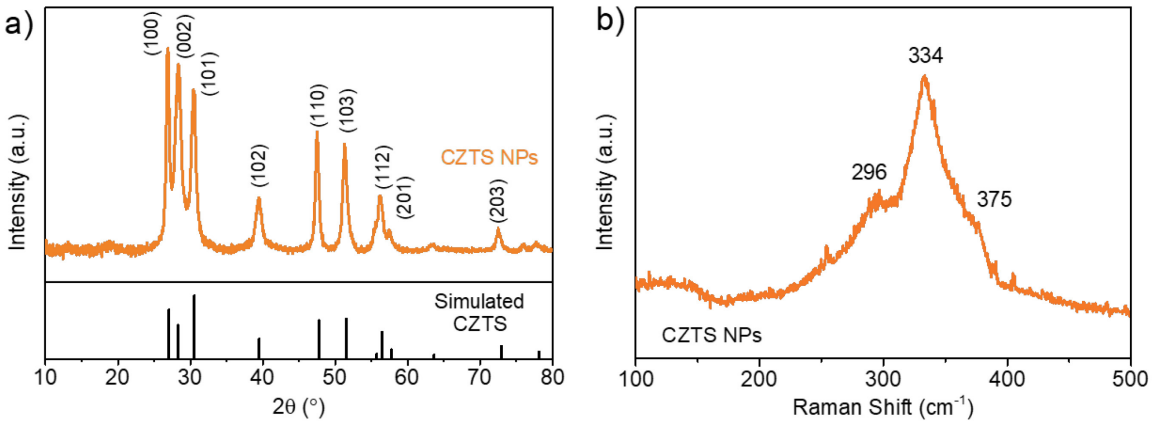

Figure 5. a) Simulated wurtzite CZTS standard as compared to CZTS nanoparticles synthesized in this work, b) Raman spectrum of CZTS nanoparticles.

In summary, we have developed a novel method of nanoparticle synthesis in which metal sulfide nanoparticles can be synthesized with inorganic sulfide and thermally degradable thioacetamide ligands directly, bypassing the need for complex and solvent intensive ligand exchange procedures. Syntheses of phase-pure $CuInS_2$ and Cu_2ZnSnS_4 nanoparticles were demonstrated, and we believe these methods can easily be extended to other metal sulfide nanomaterials. Non-toxic ink formulation in dimethyl sulfoxide and subsequent scalable blade coating and selenization yielded carbon-free absorber layers of $CuIn(S,Se)_2$, which when completed into devices, reached power conversion efficiencies of 7.1%, demonstrating the promise of this system for implantation into large scale, low toxicity photovoltaics manufacturing.

Associated Content

Supporting Information available:
Experimental methods, additional characterization data like high resolution transmission electron microscopy (HRTEM), UV-Vis absorption spectroscopy, profilometry, FTIR, thermogravimetric analysis (TGA), scanning electron microscopy.

Acknowledgements

The authors would like to acknowledge the funding support provided by the National Science Foundation under grant #1735282-NRT (SFEWS) and grant #10001536 (INFEWS). Authors would also like to thank Daniel Hayes for running TGA and providing molybdenum coated soda lime glass for photovoltaic device fabrication, Xianyi Hu for simulating the reference wurtzite CZTS spectrum, and Shubhanshu Agarwal for the collection of plan-view SEM images.

References:

(1) Nakamura, M.; Yamaguchi, K.; Kimoto, Y.; Yasaki, Y.; Kato, T.; Sugimoto, H. Cd-Free Cu(In,Ga)(Se,S)$_2$ Thin-Film Solar Cell with Record Efficiency of 23.35%. *IEEE J. Photovoltaics* **2019**, *9* (6), 1863–1867. https://doi.org/10.1109/JPHOTOV.2019.2937218.

(2) Zhang, T.; Yang, Y.; Liu, D.; Tse, S. C.; Cao, W.; Feng, Z.; Chen, S.; Qian, L. High Efficiency Solution-Processed Thin-Film Cu(In,Ga)(Se,S)$_2$ Solar Cells. *Energy Environ. Sci.* **2016**, *9* (12), 3674–3681. https://doi.org/10.1039/C6EE02352E.

(3) Bob, B.; Lei, B.; Chung, C.-H.; Yang, W.; Hsu, W.-C.; Duan, H.-S.; Hou, W. W.-J.; Li, S.-H.; Yang, Y. The Development of Hydrazine-Processed Cu(In,Ga)(Se,S)$_2$ Solar Cells. *Adv. Energy Mater.* **2012**, *2* (5), 504–522. https://doi.org/10.1002/aenm.201100578.

(4) Zhang, R.; Szczepaniak, S. M.; Carter, N. J.; Handwerker, C. A.; Agrawal, R. A Versatile Solution Route to Efficient $Cu_2ZnSn(S,Se)_4$ Thin-Film Solar Cells. *Chem. Mater.* **2015**, *27* (6), 2114–2120. https://doi.org/10.1021/cm504654t.

(5) Zhang, R.; Cho, S.; Lim, D. G.; Hu, X.; Stach, E. A.; Handwerker, C. A.; Agrawal, R. Metal–Metal Chalcogenide Molecular Precursors to Binary, Ternary, and Quaternary Metal Chalcogenide Thin Films for Electronic Devices. *Chem. Commun.* **2016**, *52* (28), 5007–5010. https://doi.org/10.1039/C5CC09915C.

(6) Zhao, X.; Lu, M.; Koeper, M. J.; Agrawal, R. Solution-Processed Sulfur Depleted Cu(In, Ga)Se $_2$ Solar Cells Synthesized from a Monoamine–Dithiol Solvent Mixture. *J. Mater. Chem. A* **2016**, *4* (19), 7390–7397. https://doi.org/10.1039/C6TA00533K.

(7) Zhao, X.; Deshmukh, S. D.; Rokke, D. J.; Zhang, G.; Wu, Z.; Miller, J. T.; Agrawal, R. Investigating Chemistry of Metal Dissolution in Amine-Thiol Mixtures and Exploiting It toward Benign Ink Formulation for Metal Chalcogenide Thin Films. *Chem. Mater.* **2019**, *31* (15), 5674–5682. https://doi.org/10.1021/acs.chemmater.9b01566.

(8) Jiang, J.; Giridharagopal, R.; Jedlicka, E.; Sun, K.; Yu, S.; Wu, S.; Gong, Y.; Yan, W.; Ginger, D. S.; Green, M. A.; Hao, X.; Huang, W.; Xin, H. Highly Efficient Copper-Rich Chalcopyrite Solar Cells from DMF Molecular Solution. *Nano Energy* **2020**, *69*, 104438. https://doi.org/10.1016/j.nanoen.2019.104438.

(9) Zhao, Y.; Yuan, S.; Kou, D.; Zhou, Z.; Wang, X.; Xiao, H.; Deng, Y.; Cui, C.; Chang, Q.; Wu, S. High Efficiency CIGS Solar Cells by Bulk Defect Passivation through Ag Substituting Strategy. *ACS Appl. Mater. Interfaces* **2020**, *12* (11), 12717–12726. https://doi.org/10.1021/acsami.9b21354.

(10) Guo, Q.; Ford, G. M.; Agrawal, R.; Hillhouse, H. W. Ink Formulation and Low-Temperature Incorporation of Sodium to Yield 12% Efficient $Cu(In,Ga)(S,Se)_2$ Solar Cells from Sulfide Nanocrystal Inks. *Prog. Photovoltaics Res. Appl.* **2013**, *21* (1), 64–71. https://doi.org/10.1002/pip.2200.

(11) McLeod, S. M.; Hages, C. J.; Carter, N. J.; Agrawal, R. Synthesis and Characterization of 15% Efficient CIGSSe Solar Cells from Nanoparticle Inks. *Prog. Photovoltaics Res. Appl.* **2015**, *23* (11), 1550–1556. https://doi.org/10.1002/pip.2588.

(12) Eeles, A.; Arnou, P.; Bowers, J. W.; Walls, J. M.; Whitelegg, S.; Kirkham, P.; Allen, C.; Stubbs, S.; Liu, Z.; Masala, O.; Newman, C.; Pickett, N. High-Efficiency Nanoparticle Solution-Processed $Cu(In,Ga)(S,Se)_2$ Solar Cells. *IEEE J. Photovoltaics* **2018**, *8* (1), 288–292. https://doi.org/10.1109/JPHOTOV.2017.2762581.

(13) McLeod, S.; Alruqobah, E.; Agrawal, R. Liquid Assisted Grain Growth in Solution Processed $Cu(In,Ga)(S,Se)_2$. *Sol. Energy Mater. Sol. Cells* **2019**, *195*, 12–23. https://doi.org/10.1016/j.solmat.2019.02.020.

(14) Deshmukh, S. D.; Ellis, R. G.; Sutandar, D. S.; Rokke, D. J.; Agrawal, R. Versatile Colloidal Syntheses of Metal Chalcogenide Nanoparticles from Elemental Precursors Using Amine-Thiol Chemistry. *Chem. Mater.* **2019**, *31* (21), 9087–9097. https://doi.org/10.1021/acs.chemmater.9b03401.

(15) Ellis, R. G.; Vak, D.; Chesman, A. S. R.; Agrawal, R. Slot Die Coating of CIGS Nanoparticle Inks for Scalable Solution Processed Photovoltaics. In *Conference Record of the IEEE Photovoltaic Specialists Conference*; 2019; pp 1830–1833. https://doi.org/10.1109/PVSC40753.2019.8980504.

(16) Alruqobah, E. H.; Agrawal, R. Potassium Treatments for Solution-Processed $Cu(In,Ga)(S,Se)_2$ Solar Cells. *ACS Appl. Energy Mater.* **2020**, *3* (5), 4821–4830. https://doi.org/10.1021/acsaem.0c00422.

(17) Ellis, R. G.; Turnley, J. W.; Rokke, D. J.; Fields, J. P.; Alruqobah, E. H.; Deshmukh, S. D.; Kisslinger, K.; Agrawal, R. Hybrid Ligand Exchange of $Cu(In,Ga)S_2$ Nanoparticles for Carbon Impurity Removal in Solution-Processed Photovoltaics. *Chem. Mater.* **2020**, *32*, 5091–5103. https://doi.org/10.1021/acs.chemmater.0c00966.

(18) Van Embden, J.; Chesman, A. S. R.; Jasieniak, J. J. The Heat-up Synthesis of Colloidal

Nanocrystals. *Chemistry of Materials*. American Chemical Society April 14, 2015, pp 2246–2285. https://doi.org/10.1021/cm5028964.
(19) Coughlan, C.; Ibáñez, M.; Dobrozhan, O.; Singh, A.; Cabot, A.; Ryan, K. M. Compound Copper Chalcogenide Nanocrystals. *Chem. Rev.* **2017**, *117* (9), 5865–6109. https://doi.org/10.1021/acs.chemrev.6b00376.
(20) Martin, T. R.; Katahara, J. K.; Bucherl, C. N.; Krueger, B. W.; Hillhouse, H. W.; Luscombe, C. K. Nanoparticle Ligands and Pyrolized Graphitic Carbon in CZTSSe Photovoltaic Devices. *Chem. Mater.* **2016**, *28* (1), 135–145. https://doi.org/10.1021/acs.chemmater.5b03426.
(21) Hages, C. J.; Koeper, M. J.; Miskin, C. K.; Brew, K. W.; Agrawal, R. Controlled Grain Growth for High Performance Nanoparticle-Based Kesterite Solar Cells. *Chem. Mater.* **2016**, *28* (21), 7703–7714. https://doi.org/10.1021/acs.chemmater.6b02733.
(22) Rehan, S.; Kim, K. Y.; Han, J.; Eo, Y. J.; Gwak, J.; Ahn, S. K.; Yun, J. H.; Yoon, K. H.; Cho, A.; Ahn, S. J. Carbon-Impurity Affected Depth Elemental Distribution in Solution-Processed Inorganic Thin Films for Solar Cell Application. *ACS Appl. Mater. Interfaces* **2016**, *8* (8), 5261–5272. https://doi.org/10.1021/acsami.5b10789.
(23) Luther, J. M.; Law, M.; Song, Q.; Perkins, C. L.; Beard, M. C.; Nozik, A. J. Structural, Optical, and Electrical Properties of Self-Assembled Films of PbSe Nanocrystals Treated with 1,2-Ethanedithiol. *ACS Nano* **2008**, *2* (2), 271–280. https://doi.org/10.1021/nn7003348.
(24) Sayevich, V.; Guhrenz, C.; Dzhagan, V. M.; Sin, M.; Werheid, M.; Cai, B.; Borchardt, L.; Widmer, J.; Zahn, D. R. T.; Brunner, E.; Lesnyak, V.; Gaponik, N.; Eychmüller, A. Hybrid *N* -Butylamine-Based Ligands for Switching the Colloidal Solubility and Regimentation of Inorganic-Capped Nanocrystals. *ACS Nano* **2017**, *11* (2), 1559–1571. https://doi.org/10.1021/acsnano.6b06996.
(25) Gabka, G.; Bujak, P.; Giedyk, K.; Kotwica, K.; Ostrowski, A.; Malinowska, K.; Lisowski, W.; Sobczak, J. W.; Pron, A. Ligand Exchange in Quaternary Alloyed Nanocrystals - a Spectroscopic Study. *Phys. Chem. Chem. Phys.* **2014**, *16* (42), 23082–23088. https://doi.org/10.1039/c4cp03850a.
(26) Kovalenko, M. V.; Scheele, M.; Talapinl, D. V. Colloidal Nanocrystals with Molecular Metal Chalcogenide Surface Ligands. *Science (80-.).* **2009**, *324* (5933), 1417–1420. https://doi.org/10.1126/science.1170524.
(27) Nag, A.; Kovalenko, M. V; Lee, J.; Liu, W.; Spokoyny, B.; Talapin, D. V. Metal-Free Inorganic Ligands for Colloidal Nanocrystals: S^{2-}, HS^{-} , Se^{2-}, HSe^{-}, Te^{2-}, HTe^{-}, TeS_3^{2-} , OH^{-}, and NH_2^{-} as Surface Ligands. *J. Am. Chem. Soc.* **2011**, *133* (27), 10612–10620. https://doi.org/10.1021/ja2029415.
(28) Jeong, S.; Lee, B. S.; Ahn, S.; Yoon, K.; Seo, Y. H.; Choi, Y.; Ryu, B. H. An 8.2% Efficient Solution-Processed $CuInSe_2$ Solar Cell Based on Multiphase $CuInSe_2$ Nanoparticles. *Energy Environ. Sci.* **2012**, *5* (6), 7539–7542. https://doi.org/10.1039/c2ee21269b.
(29) Huang, T. J.; Yin, X.; Tang, C.; Qi, G.; Gong, H. A Low-Cost, Ligand Exchange-Free Strategy to Synthesize Large-Grained Cu_2ZnSnS_4 Thin-Films without a Fine-Grain Underlayer from Nanocrystals. *J. Mater. Chem. A* **2015**, *3* (34), 17788–17796. https://doi.org/10.1039/c5ta03640b.
(30) Hassinen, A.; Moreels, I.; De Nolf, K.; Smet, P. F.; Martins, J. C.; Hens, Z. Short-Chain Alcohols Strip X-Type Ligands and Quench the Luminescence of PbSe and CdSe Quantum Dots, Acetonitrile Does Not. *J. Am. Chem. Soc.* **2012**, *134* (51), 20705–20712. https://doi.org/10.1021/ja308861d.
(31) Ritchie, C.; Chesman, A. S. R.; Jasieniak, J.; Mulvaney, P. Aqueous Synthesis of $Cu_2ZnSnSe_4$ Nanocrystals. *Chem. Mater.* **2019**, *31* (6), 2138–2150. https://doi.org/10.1021/acs.chemmater.9b00100.
(32) Marin, R.; Skripka, A.; Huang, Y. C.; Loh, T. A. J.; Mazeika, V.; Karabanovas, V.; Chua, D. H. C.; Dong, C. L.; Canton, P.; Vetrone, F. Influence of Halide Ions on the Structure and Properties of Copper Indium Sulphide Quantum Dots. *Chem. Commun.* **2020**, *56* (22), 3341–3344. https://doi.org/10.1039/c9cc08291c.

(33) Dierick, R.; Van den Broeck, F.; De Nolf, K.; Zhao, Q.; Vantomme, A.; Martins, J. C.; Hens, Z. Surface Chemistry of $CuInS_2$ Colloidal Nanocrystals, Tight Binding of L-Type Ligands. *Chem. Mater.* **2014**, *26* (20), 5950–5957. https://doi.org/10.1021/cm502687p.
(34) Hamid, S. H.; Ali, M. A. Comparative Study of Solvents for the Extraction of Aromatics from Naphtha. *Energy Sources* **1996**, *18* (1), 65–84. https://doi.org/10.1080/00908319608908748.
(35) Choi, Y. J.; Cho, K. W.; Cho, B. W.; Yeo, Y. K. Optimization of the Sulfolane Extraction Plant Based on Modeling and Simulation. *Ind. Eng. Chem. Res.* **2002**, *41* (22), 5504–5509. https://doi.org/10.1021/ie010435a.
(36) Bak, A.; Kozik, V.; Dybal, P.; Kus, S.; Swietlicka, A.; Jampilek, J. Sulfolane: Magic Extractor or Bad Actor? Pilot-Scale Study on Solvent Corrosion Potential. *Sustainability* **2018**, *10* (10), 3677. https://doi.org/10.3390/su10103677.
(37) Yue, W.; Wei, F.; He, C.; Wu, D.; Tang, N.; Qiao, Q. L-Cysteine Assisted-Synthesis of 3D In2S3 for 3D CuInS2 and Its Application in Hybrid Solar Cells. *RSC Adv.* **2017**, *7* (60), 37578–37587. https://doi.org/10.1039/c7ra05730j.
(38) Knauf, R. R.; Lennox, J. C.; Dempsey, J. L. Quantifying Ligand Exchange Reactions at CdSe Nanocrystal Surfaces. *Chem. Mater.* **2016**, *28* (13), 4762–4770. https://doi.org/10.1021/acs.chemmater.6b01827.
(39) Petrov, K. A.; Andreev, L. N. The Chemical Properties of Thioamides. *Russ. Chem. Rev.* **1971**, *40* (6), 505–524. https://doi.org/10.1070/rc1971v040n06abeh001934.
(40) Miskin, C. K.; Yang, W. C.; Hages, C. J.; Carter, N. J.; Joglekar, C. S.; Stach, E. A.; Agrawal, R. 9.0% Efficient $Cu_2ZnSn(S,Se)_4$ Solar Cells from Selenized Nanoparticle Inks. *Prog. Photovoltaics Res. Appl.* **2015**, *23* (5), 654–659. https://doi.org/10.1002/pip.2472.
(41) Yang, W.-C.; Miskin, C. K.; Hages, C. J.; Hanley, E. C.; Handwerker, C.; Stach, E. A.; Agrawal, R. Kesterite $Cu_2ZnSn(S,Se)_4$ Absorbers Converted from Metastable, Wurtzite-Derived Cu_2ZnSnS_4 Nanoparticles. *Chem. Mater* **2014**, *26*. https://doi.org/10.1002/pip.2472.
(42) Singh, A.; Geaney, H.; Laffir, F.; Ryan, K. M. Colloidal Synthesis of Wurtzite Cu_2ZnSnS_4 Nanorods and Their Perpendicular Assembly. *J. Am. Chem. Soc.* **2012**, *134* (6), 2910–2913. https://doi.org/10.1021/ja2112146.

Table of Content:

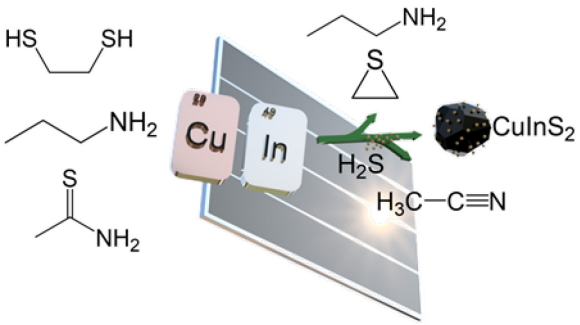

Direct Synthesis of Sulfide-Capped Nanoparticles for Carbon-Free Solution Processed Photovoltaics

Ryan G. Ellis, Swapnil D. Deshmukh, Jonathan W. Turnley, Dwi S. Sutandar, Jacob P. Fields, and Rakesh Agrawal*

Davidson School of Chemical Engineering, Purdue University, West Lafayette, IN 47907, USA

*Corresponding Author: agrawalr@purdue.edu

Supporting Information

Experimental

Materials. Copper (I) sulfide (99.99%), copper (nanopowder, 99.5% trace metals basis, ~2% oxygen), propylamine (PA; >99%), 1,2-ethanedithiol (EDT; 98%), sulfolane (99%), thioacetamide (99%), toluene (anhydrous , 99.8%), acetonitrile (99.9%, anhydrous), dimethyl sulfoxide (anhydrous, 99.9%), butylamine (99.5%), zinc (nanopowder, 99%), sodium fluoride (99.99%), cadmium sulfate hydrate (99.996%), and thiourea (>99%) were purchased from Sigma Aldrich and used as received with the exception of sulfolane, which was degassed using successive freeze-pump-thaw cycles under vacuum. Indium (99.999%), tin (99.999%), and ammonium hydroxide solution (28.0-30.0%) were purchased from Fisher Scientific and used as received. All chemicals were dispensed in an inert environment with O_2 and H_2O < 1 ppm, with the exception of cadmium sulfate hydrate, thiourea, and ammonium hydroxide. Ultrapure water was generated using a Millipore Direct-Q3 (18.2 MΩ at 25℃).

Synthesis of $CuInS_2$ and Cu_2ZnSnS_4 Nanoparticles. All synthesis work was performed under inert nitrogen or argon atmospheres. Metal precursor solutions were prepared by co-dissolving Cu and In metals in PA-EDT mixtures at 0.4M with respect to copper. A 50% excess of EDT was used assuming a minimum stoichiometry of 2 EDT per In and 1 EDT per Cu. For solutions using Cu_2S and In as precursors, separate copper and indium solutions were prepared at the same molar ratios of Cu and In with respect to EDT. These solutions were combined after all solids were dissolved. For CZTS, a minimum stoichiometry of 2 EDT per Zn and 2 EDT per Sn was assumed. When Cu_2S was used in place of Cu, separate Cu_2S and In solutions were prepared at 0.4M and mixed after complete dissolution. CIS and CZTS precursor solutions were then evaporated under vacuum, leaving isolated metal thiolate complexes. The complexes were dissolved in degassed sulfolane after stirring for 30 minutes to get a 0.4M concentration with respect to copper. For CZTS precursor solutions, 300 µL of propylamine was added to the sulfolane to help solubilize the metal thiolate complexes. Separately, thioacetamide was dissolved in 7 mL of sulfolane, where a 6:1 TAA:In and 6:1 TAA:Zn molar ratio was used. The TAA/sulfolane solution was transferred to a 100 mL 3 neck flask with a condenser, glass-sheathed thermocouple port, and a rubber septum. The TAA/sulfolane mixture was transferred to an argon purged Schlenk line where cooling water was attached to the condenser. Under stirring at 600 rpm, the TAA/sulfolane was brought to 80℃ under vacuum for 30 minutes to further degas the sulfolane and remove any trace moisture from the TAA. The reaction vessel was then backfilled with argon and brought to 200℃ for synthesis with Cu-containing precursors, and 210℃ for Cu_2S-containing precursors. Two mL of the metal thiolate in sulfolane solution was hot injected into the TAA/sulfolane solution, and the reaction was allowed to continue at the reaction temperature for 15 minutes (for Cu metal precursors), or 30 minutes (for Cu_2S precursors). The reaction mixture was naturally cooled to room temperature and precipitated using excess toluene and centrifugation. After decanting the supernatant, 4 mL of acetonitrile was used to redisperse the nanoparticles with vortex mixing. Four total centrifugation washing cycles were used, after which the supernatant was decanted, and the nanoparticles were dried under a flow of argon.

Film Coating. All coating was performed in an inert nitrogen environment. Nanoparticle thin films were prepared by dispersing the dry nanoparticles at a 200 mg/mL mass concentration in DMSO using sonication for 30 minutes. A dark viscous ink was obtained after sonication, which was then filtered through a 1 µm glass fiber filter and blade coated onto either soda-lime glass or molybdenum-coated soda-lime glass using a custom automatic blade coater. First, 12 µL of ink was dispensed on the top edge of a 1” x 2” substrate on an 80℃ heated bed. Then two passes down and up the substrate were performed at 20 mm/s using a cylindrical glass rod as a blade with a 100 µm substrate-blade gap. The films were then dried for 2 minutes at 80℃ followed by annealing at 320℃ for 1-5 minutes. Each coating yielded an approximate thickness of 400 nm. Sequential coatings were performed to reach thicknesses just over a micron. Molecular precursor films were coated directly out of dissolved solutions of Cu_2S and In in butylamine-EDT mixtures using blade coating and annealing at 300℃.

Device fabrication. After coating CIS nanoparticle films with just over a micron thickness of molybdenum coated soda-lime glass substrates, 10 nm of NaF was electron-beam evaporated onto the surface of the nanoparticle film. The film was then selenized under an argon atmosphere in a tubular furnace at 500°C along with approximately 350 mg of elemental selenium in a graphite box. After natural cooling, 50 nm of CdS was deposited on the film surface using chemical bath deposition with aqueous cadmium sulfate hydrate, thiourea, and ammonium hydroxide at 65°C. Next, i-ZnO (80 nm) and ITO (220 nm) were sputtered onto the device stack. Ni/Al (100 nm/1 μm) were electron-beam evaporated through a shadow mask to complete the device. Finally, a magnesium fluoride antireflection coating (100 nm) was deposited on top of the film. Devices were isolated by mechanical scribing with a total area of approximately 0.47 cm^2 and a grid shaded area of 4%.

Characterization. X-ray diffractograms were collected using a Rigaku SmartLab diffractometer with a 40 kV/44 mA Cu Kα (λ = 1.5406 Å) source operated at in 0.5° parallel beam (PB) mode. Raman spectra were collected on a Horiba/Jobin-Yvon HR800 Raman spectrometer at a 632.8 nm excitation laser wavelength. Transmission electron micrographs were collected using a Tecnai T20 transmission electron microscope at 200 kV accelerating voltage. Elemental ratios were determined using a Fisher XAN 250 X-ray fluorescence (XRF) instrument, running at 50 kV with a silicon drift detector, nickel filter, and helium gas purge. ^{1}H-NMR spectra were collected with a Bruker AV-III-400-HD using a relaxation time of 6 s and 32 scans. FTIR absorbance spectra were collected with a Thermo-Nicolet Nexus 670 FTIR in transmission mode on soda-lime glass or NaCl as substrates. Uniform coatings were used for absorbance measurements such that the path length between measurements was constant and therefore directly comparable before and after annealing samples. Profilometry was performed using a Dektak 6 M stylus profilometer with a 12.5 μm diameter diamond tip stylus. Thickness measurements were taken using mechanically scribed trenches. Scanning electron microscopy (SEM) images were taken using FEI Quanta 3D FEG dual-beam SEM with an Everhart− Thornley detector at an accelerating voltage of 10 kV and a working distance of 10 mm. substrates. Absorption data was collected on a thin film fabricated on soda lime glass substrate using Cary 60 UV-Vis spectrophotometer. Thermogravimetric analysis (TGA) was performed on a TA Instruments Q50 under argon atmosphere with a heating rate of 10 °C/min using an alumina sample pan on a platinum holder. J-V measurements were collected using an AM1.5G simulated solar spectrum calibrated to 1 sun intensity using a NREL calibrated silicon reference cell. The cell was placed on a 25°C temperature-controlled stage for all measurements.

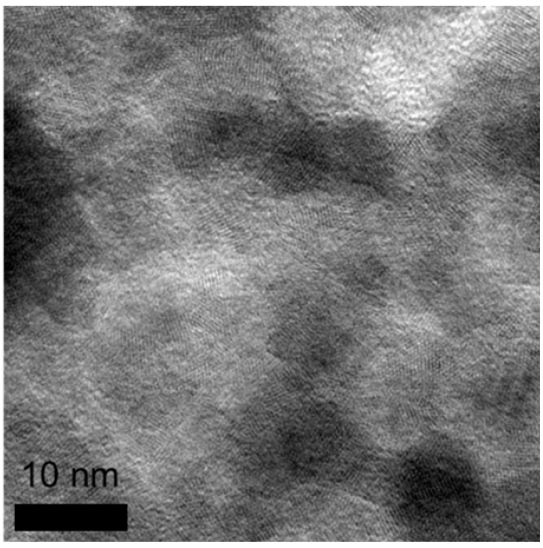

Figure S1. HRTEM of CIS nanoparticle synthesized using Cu_2S as a copper precursor

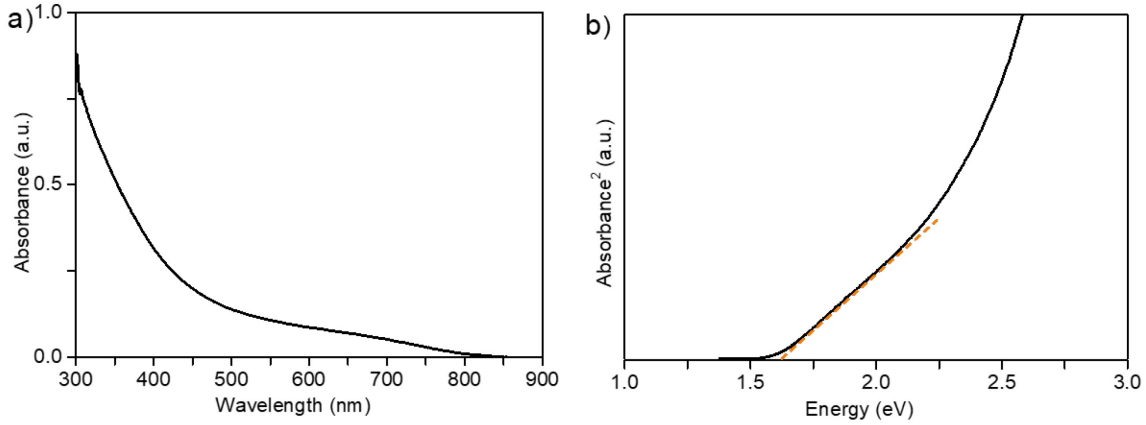

Figure S2. a) Absorption spectrum and b) Tauc plot for CIS nanoparticles prepared from Cu and In precursors.

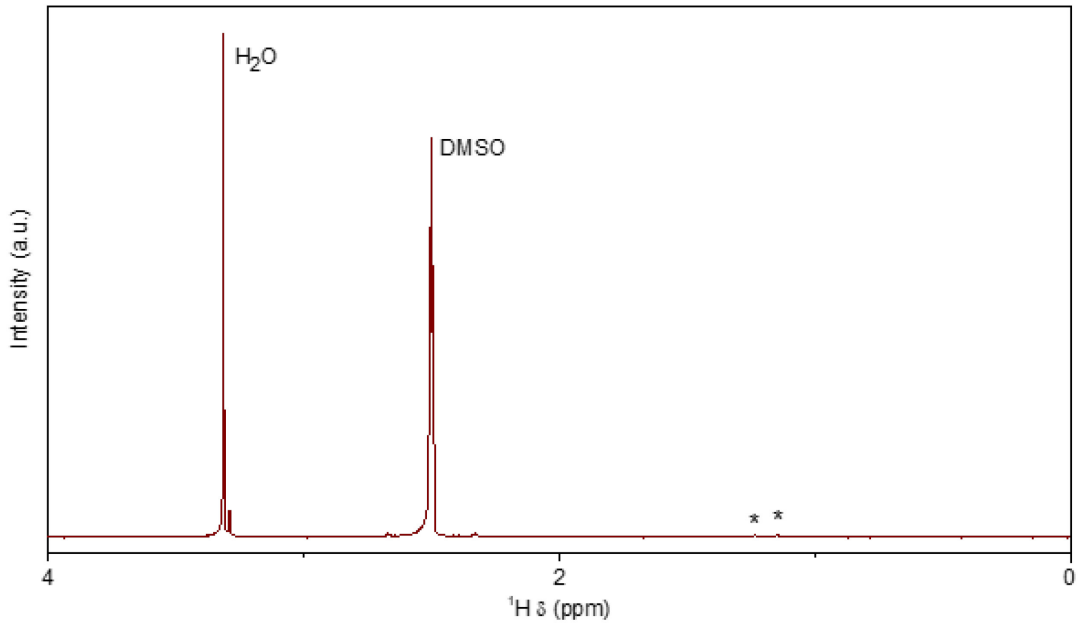

Figure S3. ^{1}H-NMR of neat as received DMSO-d6. Impurity water and residual non-deuterated DMSO are labelled along with other trace impurities marked with asterisks

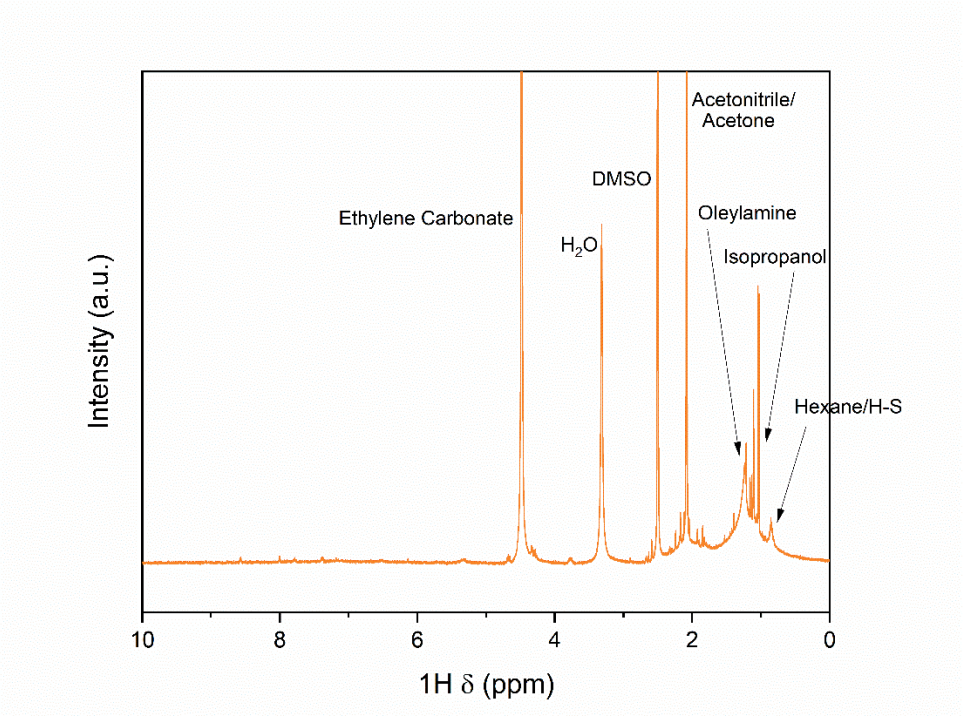

Figure S4. [1]H-NMR of diammonium sulfide capped ligand exchanged CIGS nanoparticles for reference

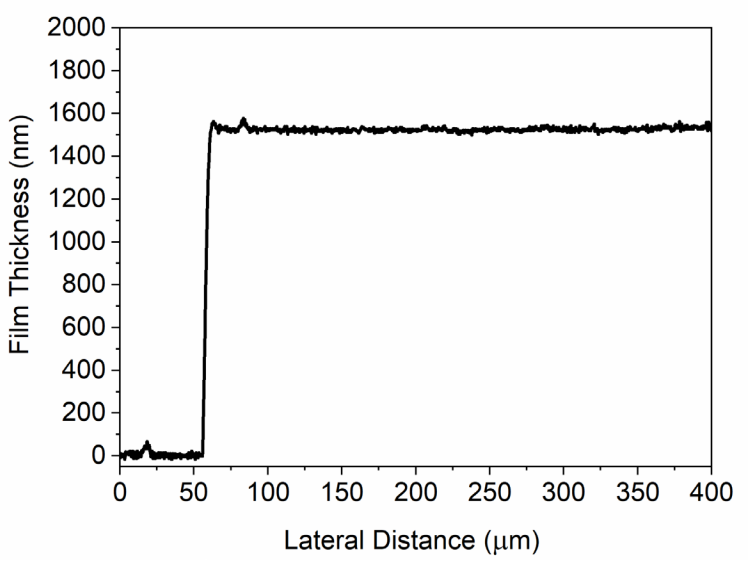

Figure S5. Profilometry scan of a CIS thin blade coated from a DMSO ink on molybdenum with a mechanically scribed trench for thickness and roughness measurement. Four successive coatings were used to reach the thickness shown.

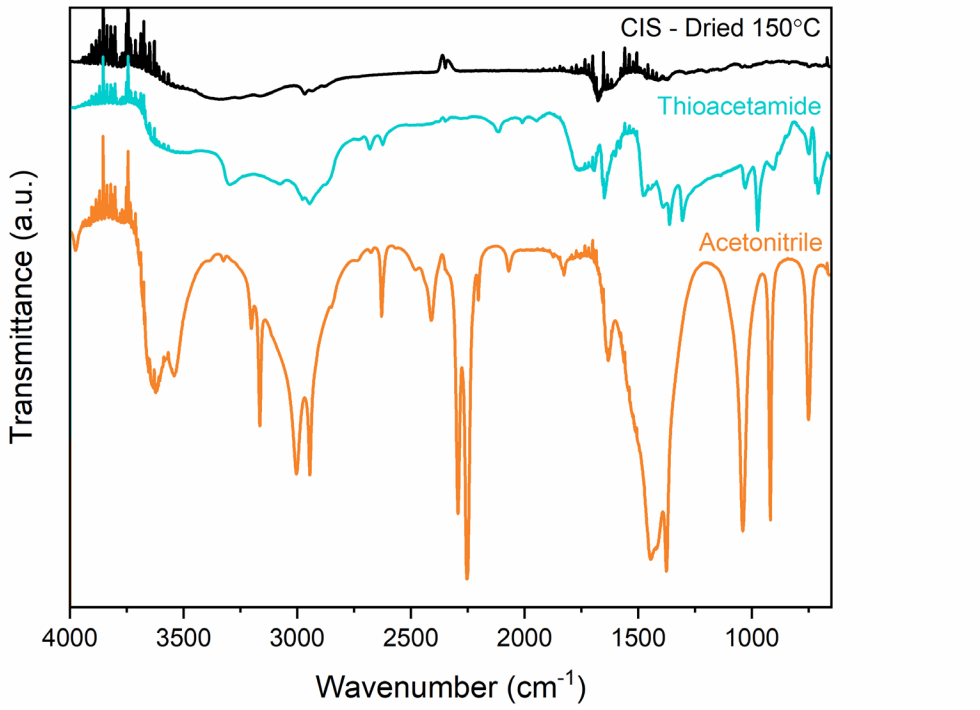

Figure S6. Full spectrum FTIR showing residual C-H and broad peaks between 3000 and 3500 cm^{-1} attributed to surface bound thioacetamide

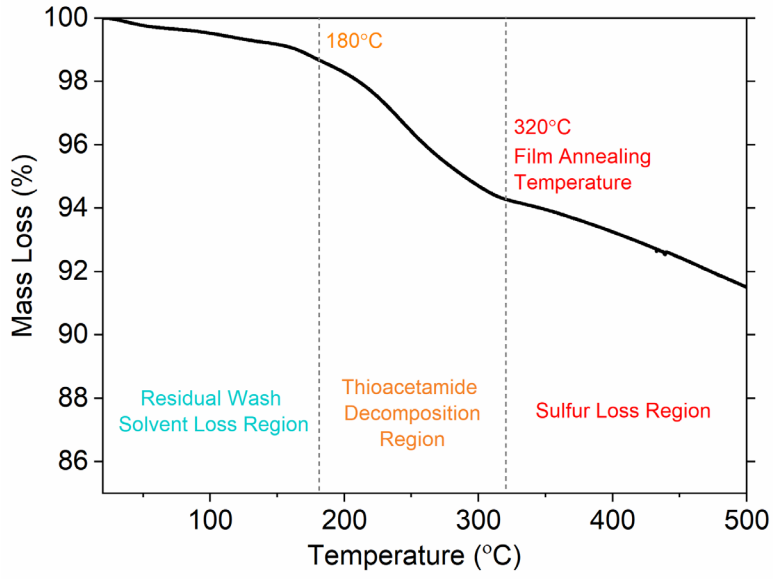

Figure S7. Thermogravametric analysis (TGA) of CIS nanoparticle prepared with Cu and In precursors demonstrating three distinct mass loss regions

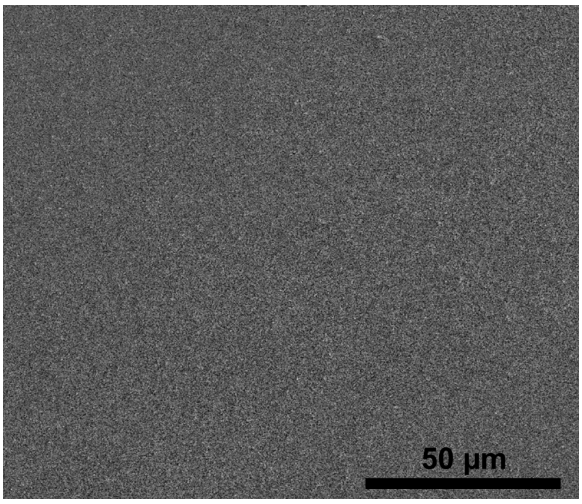

Figure S8. Low magnification plan view SEM image of a coated CIS nanoparticle film (from Cu an In precursors)

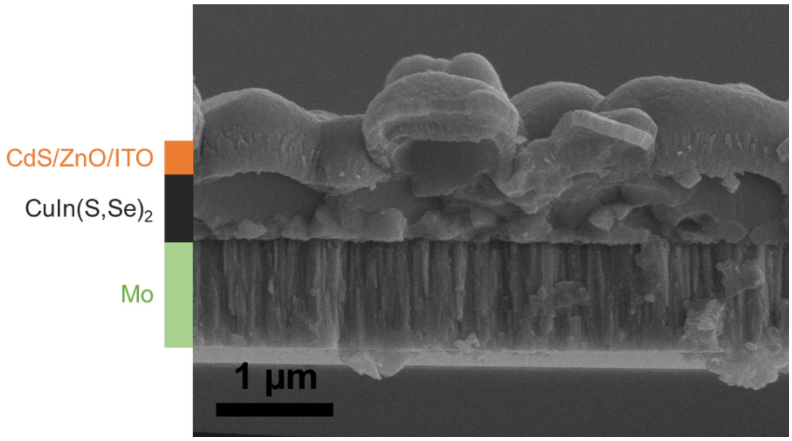

Figure S9. Cross-sectional SEM image of a complete device fabricated by selenization of direct sulfide capped CIS nanoparticle film prepared from Cu and In precursors.